High-level clonal *FGFR* amplification and response to FGFR inhibition in a translational clinical trial

Alex Pearson*[1], Elizabeth Smyth*[2], Irina S. Babina[1], Maria Teresa Herrera-Abreu[1], Noelia Tarazona[1], Clare Peckitt[2], Elaine Kilgour[3], Neil R. Smith[3], Catherine Geh[3], Claire Rooney[3], Ros Cutts[1], James Campbell[1], Jian Ning[4], Kerry Fenwick[4], Amanda Swain[4], Gina Brown[5], Sue Chua[6], Anne Thomas[7], Stephen R.D. Johnston[8], Mazhar Ajaz[9], Katherine Sumpter[10], Angela Gillbanks[2], David Watkins[2], Ian Chau[2], Sanjay Popat[11], David Cunningham[#2] and Nicholas C. Turner[#1, 8]

[1] The Breakthrough Breast Cancer Research Centre, Institute of Cancer Research, London, SW3 6JB, UK.
[2] GI Unit, Royal Marsden Hospital, Fulham Road, London, SW3 6JB, UK
[3] AstraZeneca Oncology, Macclesfield, Cheshire, SK10 4TG
[4] The Tumour Profiling Unit, Institute of Cancer Research, London, SW3 6JB, UK
[5]Department of Diagnostic Imaging, The Royal Marsden, Downs Road, Sutton, Surrey SM2 5PT
[6] Nuclear Medicine and PET/CT Department, The Royal Marsden, Downs Road, Sutton, Surrey SM2 5PT
[7] Leicester Royal Infirmary, Infirmary Square, Leicester, LE1 5WW
[8] Breast Unit, The Royal Marsden Hospital, Fulham Road, London, SW3 6JJ, UK
[9] The Royal Surrey County Hospital NHS Foundation Trust, Egerton Road, Guildford, GU2 7XX
[10] Northern Centre for Cancer Care, The Newcastle upon Tyne Hospitals NHS Foundation Trust**,** Freeman Hospital, Newcastle upon Tyne, NE7 7DN
[11] Lung Unit, The Royal Marsden, London, SW3 6JJ
*- These authors have contributed equally to the manuscript
[#]- Joint senior author

Corresponding author:

Nicholas Turner, The Institute of Cancer Research, 237 Fulham Road, London, SW3 6JB, UK, Fax: +44 (0)207 51535340, Email: nicholas.turner@icr.ac.uk

Conflict of Interest:

NCT reports receiving advisory board honoraria from Astra Zeneca. EK, NRS, CG and CR are employees of AstraZeneca Ltd and own shares in the company.

Running title: High-level clonal *FGFR2* amplification and treatment response

Abstract

FGFR1 and *FGFR2* are amplified in many tumour types, yet what determines response to FGFR inhibition in amplified cancers is unknown. In a translational clinical trial we show that gastric cancers with high-level clonal *FGFR2* amplification have a high response rate to the selective FGFR inhibitor AZD4547, whilst cancers with sub-clonal or low-level amplification did not respond. Using cell lines and patient derived xenografts models, we show high-level *FGFR2* amplification initiates a distinct oncogene addiction phenotype, characterised by FGFR2 mediated transactivation of alternative receptor kinases, bringing PI3 kinase/mTOR signalling under FGFR control. Signalling in low-level *FGFR1* amplified cancers is more restricted to MAPK signalling, limiting sensitivity to FGFR inhibition. Finally, we show circulating tumour DNA screening can identify high-level clonally amplified cancers. Our data provides a mechanistic understanding of the distinct pattern of oncogene addiction seen in highly-amplified cancers and demonstrate the importance of clonality in predicting response to targeted therapy.

Statement of Significance

Robust single agent response is only seen in high-level *FGFR* amplified cancers, with copy number level dictating response to FGFR inhibition both *in vitro*, *in vivo,* and in the clinic. High-level amplification of *FGFR2* is relatively rare in gastric and breast cancers, and we show that screening for amplification in circulating tumour DNA may present a viable strategy to screen patients.

Introduction

Activation of the fibroblast growth factor receptors (FGFRs) is a common oncogenic mechanism, with activation of the FGFRs occurring in a subset of nearly all common cancers (1, 2). Activating genetic events in carcinomas include receptor amplification, mutation, and generation of aberrant receptor fusions through translocation (1, 2). There is limited understanding of how these diverse oncogenic events differ in their signalling to downstream pathways, and consequently whether the same or different therapeutic approaches may be required to treat cancers with different genetic events.

Amplification of *FGFR1* is found in ~10% breast cancer and ~15% squamous lung cancers, with amplification of *FGFR2* found in ~8% gastro-oesophageal cancer and ~2% breast cancer (1). We conducted a translational clinical trial to assess whether cancers with amplification of *FGFR1* or *FGFR2* respond to the selective FGFR inhibitor AZD4547 (3). Patients were screened for the presence of amplification using criteria defined for detection of *HER2* amplification (4). Through the clinical trial we identify that high-level copy number amplification is required for response to selective FGFR inhibition. Through analysis of functional genomic screens (5), we show that high level *FGFR2* amplified cell lines have a distinct oncogene addiction phenotype, that is characterized by PI3 kinase and mTOR signalling becoming dependent on FGFR signalling. We investigate the factors that predispose to oncogene addiction phenotype, and the implications for response to inhibitors targeting amplified receptor tyrosine kinases.

Results

FGFR2 amplified cancers have a high response rate to AZD4547

We assessed the activity of the FGFR selective inhibitor AZD4547 in *FGFR1* amplified breast cancer and *FGFR2* amplified gastro-oesophageal cancer. We screened 341 patients with advanced cancer by fluorescent *in situ* hybridization (FISH) for the presence of gene amplification, identifying *FGFR1* amplification in 18% advanced estrogen receptor positive breast cancer and *FGFR2* amplification in 9.0% advanced gastro-oesophageal cancer. Eight patients with *FGFR1* amplified breast cancer and nine with *FGFR2* amplified gastro-oesophageal cancer were treated with AZD4547 in a translational clinical trial (Supplementary Fig. 1A). One *FGFR1* amplified (12.5% response rate) and three *FGFR2* amplified (33% response rate) patients had confirmed responses to AZD4547 (Fig. 1A and B), reaching the predefined criteria for efficacy in the *FGFR2* amplified cohort. The responses were durable with a median progression free survival of responding patients of 6.6 months (range 6.2-10.5 months, Fig. 1A). Comparison of 18F-fludeoxyglucose positron emission tomography (FDG-PET) in responding patients between baseline and day 15 demonstrated a substantial reduction in glucose uptake in all responding *FGFR2* amplified gastric cancers, although there was no change in the *FGFR1* amplified breast cancer (Fig. 1C). The FDG-PET responses were maintained at 8 weeks (Supplementary Fig. 1B). Two additional patients with *FGFR2* amplified gastric cancer had a response in day 15 FDG-PET but did not have a confirmed response by RECIST criteria (Patients 135 and 99, Supplementary Fig. 1C). Serum phosphate was elevated from baseline in the majority of patients on the study (Supplementary Fig. 1D, P=0.0002 Wilcoxon matched pairs-signed rank test), as a pharmacodynamic marker of interrupting FGF23 signalling by FGFR inhibition (6). There was no correlation of response to change in phosphate level. Both a continuous and intermittent schedule of AZD4547 were used in the trial (methods). Of the

responders, patient 21 and 207 were treated on the intermittent schedule, and patients 269 and patient 316 received continuous treatment.

High-level clonal FGFR2 amplification is a therapeutic target for selective FGFR inhibitors

We investigated the pathological basis of response in *FGFR* amplified cancers, the relatively high response rate of *FGFR2* amplified gastric cancers compared to *FGFR1* amplified breast cancer, with FDG-PET reductions only in *FGFR2* amplified cancers. We assessed relative *FGFR* copy number by digital PCR in baseline tumour biopsies of patients treated in the clinical trial. For all patients with gastric cancer, the gastro-esophageal disease was biopsied by endoscopy. The response of the site biopsied was concordant with response with other sites of disease. Multiple different tumour sites were biopsied in patients with breast cancer. In the one patient who responded, the biopsied site responded along with other non-biopsied sites.

Cancers with high copy number (high-level) *FGFR* amplification were more likely to respond to AZD4547 (P=0.0026 Mann-Whitney U Test, Fig. 2A), with response only observed in cancers with high-level amplification in this trial. Within *FGFR2* amplified cancers, high-level amplification was associated with a substantially higher expression of both *FGFR2* mRNA and FGFR2 protein assessed by immunohistochemistry on baseline biopsies (Fig. 2B and Supplementary Fig. 2A and 2B). Truncated isoforms of FGFR2 have been shown to be potentially important for FGFR2 oncogenic transformation (7, 8). Only cancers with high-level *FGFR2* amplification had expression of the truncated FGFR2-C3 isoform although at varying levels suggesting that the C3 isoform was not critical to established cancers (Supplementary Fig. 2C). However, expression of FGFR2-C3 may have potential as a biomarker for enrichment of patients likely to respond to FGFR inhibition.

We explored the role of clonality in response to AZD4547 in *FGFR2* amplified cancers, using *in situ* heterogeneity mapping (online methods). Two responding patients had clonal homogeneously amplified tumours (>99% tumour cells *FGFR2* amplified), the third patient having insufficient residual baseline tissue to make an assessment, whereas all non-responding patients had tumours with sub-clonal heterogeneous amplification with the presence of non-amplified tumour cells (Fig. 2C). In particular, heterogeneity in *FGFR2* amplification was noted in patient 135 that had a high-level amplified tumour that did not respond to AZD4547. There was limited evidence of heterogeneity and the presence of non-amplified tumour cells in patient 99 that also did not respond. Both patient 135 and 99 had day 15 FDG-PET responses (Supplementary Fig 1C), suggesting that sub-clonality may explain the clinical pattern of FDG response that did not subsequently result in tumour shrinkage and clinical response. We compared paired gene expression between baseline and day 15 on-treatment biopsies with a custom Nanostring panel. In the heterogeneously amplified tumour from patient 135, high *FGFR2* mRNA expression was lost at day 15 (Fig. 2D), whilst in the homogeneously amplified cancers high *FGFR2* mRNA expression was maintained at day 15. Similarly, in patient 135 *FGFR2* copy number was substantially reduced at day 15 (Supplementary Fig. 2D). These findings may reflect the inherent difficulty of sampling in a heterogeneous tumour, but equally could reflect clonal selection by AZD4547. In paired gene expression analysis, the one *FGFR1* amplified cancer that responded to AZD4547 had upregulation of estrogen receptor target genes in the day 15 biopsy (Supplementary Table 1), suggesting that unregulated estrogen signalling may have limited sensitivity to the FGFR inhibitor in this tumour.

High-level *FGFR2* amplification occurred in only 5% gastric cancers (7/135, arbitrarily defined as FISH ratio>5), a prevalence that may present a barrier to future drug development. We assessed whether screening for amplification in circulating free plasma DNA could identify high-level clonal amplified cancers (9). *FGFR2* copy number was elevated in plasma DNA of all three responding patients (Fig. 2E), and also in patient 99 who

had a response in day 15 FDG-PET (Supplementary Fig. 1C). However, *FGFR2* copy number was not elevated in plasma DNA of patient 135 with the sub-clonal amplification, and not in low-level amplified cancers, suggesting that plasma assessment has potential to screen for high-level and clonal amplified cancers, to overcome the challenge posed by screening for amplifications on tumour biopsies.

High-level FGFR2 amplified cancer models are highly sensitive to FGFR inhibition

This data suggested that high-level clonal amplification, in particular for *FGFR2* amplified cancers, may be required for response to selective FGFR inhibitors, and we investigated why high-level amplification may associate with distinct addiction to FGFR signalling. We examined *FGFR* copy number in a panel of 74 cancer cell lines (n=25) and gastric tumours (n=49). A distinct bimodal pattern of *FGFR2* copy number was observed (Bimodality index 2.74, Fig. 3A), suggesting a distinct high-level *FGFR2* amplified group (10). In contrast, in a panel of 82 cancer cell lines (n=22) and breast tumours (n=60), there was a less pronounced bimodal distribution in *FGFR1* amplification (Bimodality index 1.3, Fig. 3A). This suggested that high-level amplification was seen more distinctly in *FGFR2* amplified cancers.

In a panel of *FGFR* driven cell lines (Supplementary Table 2), FGFR auto-phosphorylation (Tyr653/654 loop phosphorylation) was very substantially increased in high-level *FGFR2* amplified cell lines (Fig. 3B), suggesting that high-level *FGFR2* amplification resulted in FGFR hyper-activation, potentially reflecting the very high level of *FGFR2* copy number seen in *FGFR2* amplified cell lines (Supplementary Fig. 3A). Furthermore, *FGFR2* high level amplified cell lines were more sensitive to FGFR inhibitors AZD4547 and PD173074 *in vitro* than low-level *FGFR1* amplified cell lines*,* both in terms of lower EC50 and increased maximal effect *(*Fig. 3C and D). Similarly, *FGFR2* amplified cell lines were more sensitive to PD173074 than *FGFR2* mutant cell lines (*P*=0.0357 Mann-Whitney U Test, Supplementary Fig. 3B), and the level of CNV correlated with sensitivity to FGFR inhibition (R=0.8095,

P=0.0218, Supplementary Fig 3C). In addition, AZD4547 robustly increased caspase 3/7 activation only in *FGFR2* amplified cell lines (Fig. 3E).

To validate these findings, we established patient derived xenografts (PDX) in nude mice from the baseline biopsies of two *FGFR2* clonally amplified patients who responded to AZD4547 in the clinic (Fig. 1). To validate the models we performed whole exome sequencing was on the patient's archival diagnostic tumour biopsies, baseline tumour biopsies, germline, and on the established PDX models. There was high agreement in somatic mutations between the PDX models and the patient's baseline tumour suggesting an absence of substantial genetic drift and that the models were an accurate representation of the baseline tumour biopsy (FG42/pt316 R=0.86, FG51/pt269 R=0.85, Supplementary Fig 3D). Both PDX models, FG51 (pt269) and FG42 (pt316), were highly sensitive to AZD4547 *in vivo,* in FG51 median 70% tumour shrinkage and 2/5 complete responses, and in FG42 median 74% tumour shrinkage and 0/5 complete responses (Fig. 3F). AZD4547 induced an apoptotic response as assessed by cleaved caspase 3 on PDX tumour lysates (Fig. 3G).

High-level FGFR2 amplification initiates a distinct oncogene addiction phenotype characterised by FGFR dependent control of PI3K-AKT signalling

To investigate why high-level *FGFR2* amplified models demonstrated high sensitivity to FGFR inhibitors, we analysed a functional genomic screen of a panel of *FGFR* driven cell lines transfected with an siRNA screening library directed against the kinome and phosphatome (5). Using supervised hierarchical clustering we identified the siRNAs that selectively modified sensitivity to the FGFR inhibitor PD173074 (5) in *FGFR2* amplified cell lines, compared to other FGFR driven cell lines, identifying a distinct set of siRNAs that was strongly enriched for components of the PI3K pathway and canonical NFκB signalling (Fig. 4A and Supplementary Fig. 4A). Increased sensitivity to FGFR inhibition was confirmed with multiple different siRNA for NFκB signalling pathway components IKBKB and MAP3K7

(Supplementary Fig. 4B). PTEN siRNA reduced the sensitivity of *FGFR2* amplified cell lines to PD173074 with little effect in other *FGFR* driven cell lines (Fig. 4A and Supplementary Fig. 4A, *P*=0.009 Mann Whitney U Test). In validation work, PTEN silencing reduced the sensitivity of *FGFR2* amplified breast cancer cell line SUM52 to PD173074 in clonogenic assays (Fig. 4B), induced AKT phosphorylation, and increased the concentration of PD173074 required to inhibit AKT phosphorylation (Fig. 4C).

These data suggested that *FGFR2* amplified cell lines may show a distinct reliance on PI3 kinase signalling compared to other FGFR driven cell lines. Interestingly in gastric cancer TCGA data, *PIK3CA* mutation occurred in 23% (48/206) non-amplified cancers, and in 0% (0/13, p=0.036 Fishers exact test) *FGFR2* amplified cancers, suggesting distinct mechanisms of PI3 kinase pathway activation (11). We studied downstream signalling in response to PD173074 across a panel of FGFR driven cell lines (Fig. 4D and Supplementary Fig. 4C). Phosphorylation of ERK1/2 was reduced in all cell lines by PD173074 (Fig. 4D and Supplementary Fig. 4C) in keeping with the physiological effects of FGFR signalling through the MEK-ERK pathway (1). In contrast, only in *FGFR2* amplified cell lines was AKT Ser473 phosphorylation reduced by PD173074, with no reduction in *FGFR1* amplified cell lines as well as minimal reduction in *FGFR2* and *FGFR3* mutant cell lines (Fig. 4D and Supplementary Fig. 4C). In *FGFR1* amplified cell lines, PD173074 also had little effect on AKT Thr308 or PDK1 Ser241 phosphorylation (Supplementary Fig. 4D). We established *in vitro* primary spheroid cultures from *FGFR2* amplified PDXs FG51 (pt269) and FG42 (pt316). In these primary spheroid cultures, AZD4547 inhibited AKT phosphorylation (Fig. 4E) suggesting a similar pattern of FGFR dependent PI3K signalling was seen in patient derived material.

AZD4547 inhibited 4EBP1 phosphorylation in *FGFR2* amplified cell lines (Fig. 4F) and PDX derived spheroids (Fig. 4E), suggesting that mTOR signalling was substantially inhibited by FGFR inhibition. In contrast, AZD4547 had minimal effect on 4EBP1 phosphorylation in *FGFR1* amplified cell lines (Fig. 4F). AZD4547 decreased levels of phospho-S6 in both

FGFR1 (2/3) and *FGFR2* (2/3) amplified cell lines, in keeping with the potential regulation of S6 phosphorylation by MEK-ERK MAPK signalling (Supplementary Fig. 4E). In *FGFR1* amplified cell lines inhibition of mTOR was synergistic with FGFR inhibition (Supplementary Fig.4F), converting a cytostatic effect of FGFR inhibition alone to a cytotoxic effect (Supplementary Fig. 4G), illustrating the importance of mTOR inhibition in initiating a cytotoxic response. Finally, in *FGFR2* amplified cell lines AZD4547 inhibited eIF4G loading onto 7methyl GTP (Fig. 4G) and inhibited nascent protein synthesis determined using incorporation of the methionine analog L-azidohomoalanine (Fig. 4H), demonstrating inhibition of mTOR signalling and cap dependent translation.

Amplified FGFR2 activates PI3 kinase in part through transactivation of multiple alternative receptor tyrosine kinases.

We set out to determine how PI3 kinase signalling becomes FGFR dependent in highly amplified cell lines. FGFRs signal to PI3 kinase in a canonical fashion through binding of the FGFR specific adapter protein FRS2 to GRB2 and GAB1 (12). Silencing GRB2 modestly increased AKT phosphorylation in the SUM52 *FGFR2* amplified cell line, and silencing FRS2α resulted in only a minor reduction of AKT phosphorylation (Supplementary Fig. 5A-B). In addition the PI3 kinase regulatory subunit p85 (PIK3R1) did not appear to associate with FGFR2 as assayed by immunoprecipitation (Fig. 5A), suggesting that FGFR2 signalling controlled PI3 kinase signalling through a non-canonical mechanism.

To explore how FGFR2 activated PI3 kinase, we assessed the phosphorylation of 49 receptor tyrosine kinases (RTK) in response to FGFR inhibition, noting reduced tyrosine phosphorylation of all receptor tyrosine kinases assayed in SUM52 (Fig. 5B), and FGFR3, ERBB3 and partially EGFR in the *FGFR2* amplified gastric cancer SNU16 cell line (Fig. 5B). Similarly in PDX model FG42 (pt316) there was a similar pattern of phosphorylation of FGFR2, EGFR and ERBB3, with substantial reduction in phosphorylation of all RTKs to

FGFR inhibition in RTK arrays and by western blot (Figure 5C). In contrast, PD173074 treatment had little effect on RTK phosphorylation in the *FGFR1* amplified cell line JMSU1 (Supplementary Fig. 5C). Phosphorylation of ERBB3 Tyr1289 and EGFR Tyr1068 was inhibited by PD173074 in *FGFR2* amplified cell lines (Supplementary Fig. 5D), with ERBB3 phosphorylation unaffected by inhibition of EGFR/HER2 with gefitinib or lapatinib (Supplementary Fig. 5E).

The interaction between ERBB3 and p85 PI3K assayed by immunoprecipitation was inhibited by PD173074 (Fig. 5D), and silencing of *ERBB3* with multiple different siRNA partially reduced AKT phosphorylation in SUM52 and in SNU16 (Fig. 5E). ERBB3 was not observed to interact with FGFR2, suggesting that FGFR2 may not phosphorylate ERBB3 directly (Fig. 5D). Among a panel of cell lines, SNU16 were observed to have high expression of IGF1R (Supplementary Fig. 5F). In contrast to ERBB3, IGF1R phosphorylation was not decreased by PD173074 in SNU16 (Fig. 5B and 5F), whilst inhibition of IGF1R with AEW541 also blocked AKT phosphorylation (Fig. 5G) at concentrations that had no effect on FGFR2 auto-phosphorylation (Supplementary Fig. 5G). Similarly, levels of AKT phosphorylation were decreased by knockdown of IGF1R using siRNA (Supplementary Fig 5H). Therefore, both FGFR2 and IGF1R signalling were necessary for signalling to PI3K-AKT in SNU16. Activation of PI3 kinase catalytic activity requires binding of GTP bound RAS to p110α, or GTP bound CDC42/RAC1 to p110β (13), and release from inhibitory effects of the p85 regulatory subunit (14). Inhibition of FGFR signalling with PD173074, not IGF1R signalling with AEW541, reduced RAS activation in SNU16 (Fig. 5H). Conversely, p85 PI3K that did not associate with FGFR2 (Fig. 5A), bound to IRS1 in an IGF1R kinase dependent fashion (Fig. 5I). Therefore PI3 kinase pathway signalling is activated through the combined effects of FGFR2 dependent activation of RAS, and p85 binding to ERBB3 and IGF1R/IRS1. FGFR2 signalling trans-phosphorylates ERBB3 to act as a scaffold to bind p85, with IGF1R signalling promoting IRS1 binding to p85, to thereby activate PI3 kinase signalling.

Discussion

The diversity of mechanisms through which FGFR signalling are activated in cancer present a clinical translational challenge, how similar or dissimilar are the different mechanisms of activating FGFR signalling? With a translational clinical trial we identify that cancers with high-level *FGFR2* amplification form a distinct group characterized by a strong oncogene addiction phenotype and high sensitivity to AZD4547. High-level amplification initiates distinct signalling characterized by transactivation of alternative receptor tyrosine kinases to bring PI3 kinase and mTOR signalling under control of FGFR2.

Our study has implications for targeting amplified receptor tyrosine kinases (RTKs). The archetypal model for targeting amplified RTKs is that of *HER2* amplification in breast cancer (15), where the level of *HER2* amplification does not affect sensitivity to the HER2 targeting antibody trastuzumab (16). Our data suggests that *HER2* amplification in breast cancer may be a limited model for targeting other amplified RTKs, and that criteria developed to identify cancers sensitive to HER2 targeting (a *HER2* to centromere copy number ratio of >=2, and/or absolute HER2 copy number >=6) may not necessarily translate to other RTKs. HER2 has unique biology amongst RTKs, lacking an activating ligand and with inherent potential for constitutive activation when over-expressed, and a very tight relationship between the presence of amplification of any copy number level and overexpression of HER2 (17). In contrast, high-level *FGFR* copy number amplification associates with sensitivity to FGFR inhibition, with high-level amplification resulting in high expression of FGFR2 initiates a distinct oncogene addiction phenotype. In addition, low-level *FGFR1/2* amplification does not strongly associate with FGFR over-expression (4). Our data strongly suggests that clinical trials targeting FGFR, and potentially other RTKs, should consider higher thresholds for amplification. We also demonstrate the importance of assessing amplification clonality in predicting durable responses to therapy, the potential to assess the degree of heterogeneity using automated *in situ* heterogeneity mapping of FISH, and that it may be possible to identify patients with highly *FGFR2* amplified gastric cancers by analysis

of *FGFR2* copy number in cell free plasma DNA, providing a potential simple strategy to screen patients for rare amplifications.

We show that high-level *FGFR2* amplification initiates an oncogene addiction phenotype in part through activation of alternative receptor kinases that brings PI3 kinase pathway signalling under the control of FGFR signalling. FGFR2 lacks consensus binding sites for the PI3 kinase p85 regulatory subunit, and we show that over-expressed FGFR2 activates PI3 kinase signalling indirectly through cooperation with other RTKs including ERBB3 (18) and IGF1R. FGFR2 trans-phosphorylates ERBB3, via a mechanism not identified in these studies, to promote binding to p85 PI3K, with ERBB3 acting as a scaffold protein. In contrast, FGFR2 cooperates with IGF1R in a related but distinct fashion, where FGFR2 promotes PI3 kinase signalling through RAS activation while IGF1R signalling promotes p85 binding via IRS1 (Supplementary Fig. 6). For lower-level *FGFR1* amplified cell lines PI3 kinase and mTOR signalling is not blocked by FGFR inhibition and this limits the sensitivity of these cell lines to FGFR inhibition, characterised by a lack of FGD-PET changes seen in the *FGFR1* amplified responding patient in our clinical-translational trial. Both PI3 kinase and mTOR inhibitors synergise with FGFR inhibition in these cell lines (Supplementary Fig.4), identifying a potential combination strategy for *FGFR1* amplified cancers that do not exhibit a strong oncogene addiction phenotype that can be investigated in future research.

In this study we identify the importance of high-level clonal amplification in predicting response to FGFR selective inhibitors. High-level amplifications are of relatively low prevalence and we show that high-level clonal *FGFR2* amplification can be detected through ctDNA screening, opening up a screening strategy to facilitate future development of drugs targeting amplified receptor tyrosine kinases.

Grant Support

This research has been supported by Cancer Research UK grant C30746/A16642.

Acknowledgments

NCT acknowledges generous support from both Breast Cancer Now and from the Mary-Jean Mitchell Green Foundation. ES, GB, SC, IC, SP, DC and NCT acknowledge the support of the NIHR ICR/RMH biomedical research centre. We acknowledge the generous donation of the Birk and Katri families to the RMH Research fund.

Methods

Clinical Trial Design

The *FGFR* trial (EudraCT No.:2011-003718-18) is a phase II, open label, non-randomised study of AZD4547 in patients with previously treated advanced *FGFR* amplified cancer. Written informed consent was obtained from all patients. The study was carried out in accordance with the Declaration of Helsinki and approved by local institutional review boards. The study originally consisted of three independent tumour cohorts (*FGFR*1 amplified breast and squamous NSCLC and *FGFR*2 amplified gastroesophageal cancer), however due to poor accrual the lung cohort was closed to further recruitment. *FGFR* amplification testing was performed centrally on archival tissue and an *FGFR* ratio of ≥2.0 (FGFR1:CEP8 and FGFR2:CEP10) was required for study entry. Prior to treatment patients underwent a biopsy and PET-CT, repeated on study between day 10-14. Treatment consisted of AZD4547 80mg twice daily (initially on an intermittent schedule of two weeks on, one week off which was subsequently amended to continuous dosing). Primary endpoint was confirmed overall response rate. The study followed a Simon 2 stage, optimal design. One or more responses were required in the initial 9 patients in each cohort, to recruit a total of 17 patients. Three of more patients were required to conclude that cohort had sufficient efficacy for further study.

Cell lines and materials

Bladder cells lines (RT112M, MGHU3, JMSU1, 97.7, 94.10) were from the laboratory of MA Knowles (19) in 2010. Ocum2M were obtained from the laboratory of Masakazu Yashiro (Department of Surgical Oncology, Osaka City University Graduate School of Medicine) in 2010. All other cell lines were from the laboratory of A Ashworth in 2014 (Gene Function, Institute of Cancer Research, London). CAL120, MFE-296, MFE280, Kato III and An3CA

were originally obtained from CTS cell line service. BT-20, BT-483, BT549, CAMA1, DMS114, Hs578T, HCC1143, MDAMB134, MDAMB157, MDAMB175, MDAMB231, MDAMB361, MDAMB453, MCF12A, NCI-H1581, NCI-H520, T47D and ZR-75-1 were originally obtained from ATCC. MFM223, SUM44, SUM52, SUM149, and Snu16 were originally from Asterand. All cell lines were banked in multiple aliquots on receipt to reduce risk of phenotypic drift, and identity confirmed by STR profiling with the PowerPlex 1.2 System (Promega). Cultured cell lines were subjected to STR profiling after approximately 20 passages. In addition, cultured cell lines were tested once per month for the presence of mycoplasma. Cell lines were maintained in phenol red free DMEM, DMEM/F12, or RPMI with 10% FBS (PAA gold) and 2mM L-glutamine (Sigma-Aldrich, Dorset, UK).

Antibodies used were phosphorylated AKT-Ser473 (4058), p-AKT T308 (2965), AKT (4691), phospho-4EBP1 T37/46 (2855), 4EBP1 (9452), phospho-ERK1/2-Thr202/Tyr204 (4370), ERK1,2 (9102), EGFR (2232), phospho-EGFR-Y1068 (3777), phospho-ERBB3-Y1289 (4791), phospho-ERBB2-Y1221/1222 (2249), phospho-FGFR Y653/654 (3471), phospho-FRS2a (3864), phospho-IGF1R (3918), IGF1R (9750), p85 PI3K (4292), PIK3CA (4255), PTEN (9559), phospho-ribosomal protein S6 (5364), ribosomal protein S6 (2217) (all Cell Signalling Technology, Danvers, MA). βactin (A5441) (Sigma). FGFR2 (sc-122), EGFR (sc-03), PARP1 (sc-8003), and FRS2 (sc-8318) (Santa-Cruz Biotechnology, Santa Cruz, CA). ERBB3 (ab32121), and FGFR1 (ab76464) (Abcam). Grb2 (610111, BD Transduction Laboratories). p85 PI3K (ABS233, Millipore). AZD4547 and AZD8055 were provided by Astra Zeneca. CI-1040, GDC0941, KU0063794 and rapamycin were purchased from Selleckchem. PD173074 was from Sigma, gefitinib from Tocris. NVP-AEW541 from Cayman Chemicals. siRNA were from Dharmacon, Non-Targeting siRNA Pool#2, PTEN (MU-003023-02) set of 4, PLK1 (siPLK1, M-003290-01), FR2Sa (MU-006440-02) set of 4, Grb2 (MU-019220-00) set of 4, ErbB3 (MU-003127-03) set of 4 and IGF1R (MU-003012-05) set of 4. siRNA against IKBKB and MAP7K3 were obtained from Dharmacon as part of a custom validation panel.

Tumour samples

Additional tumour samples for analysis were obtained from existing trials. Gastric cancers (n=40) were from the MAGIC Trial (20). Breast cancers (n=42) were from tissue collection studies approved by multi-centre research ethics committees (ref.nos. 10/H0805/50 and 11/LO1595). Written informed consent was obtained from all patients. The study was carried out in accordance with the Declaration of Helsinki and approved by local institutional review boards.

Purification of DNA and RNA

DNA and RNA was extracted from fresh frozen tumour samples using AllPrep™ micro DNA/RNA extraction kit (QIAgen 80284) and from FFPE tumour samples using AllPrep™ DNA/RNA FFPE extraction kit (QIAgen 80234). In both cases a section was stained with haematoxylin and eosin and tumour marked out by a pathologist. Sections were cut and stained with nuclear fast red and tumour macrodissected prior to nucleic acid extraction using the appropriate kit. Plasma DNA was extracted from 2ml of plasma using QIAamp® Circulating Nucleic Acid kit (QIAGEN 55114) according to the manufacturer's guidelines.

Purified RNA was quantified using the Qubit® RNA HS Assay kit (Life Technologies, Q32855). Purified DNA was quantified using the Qubit® dsDNA HS Assay kit (Life Technologies, Q32854). Plasma DNA was quantified by ddPCR using the *RPPH1* CNV reference assay to calculate copies/well and multiplying by the c-value (3.3pg), an estimate of the mass of a single haploid human genome.

Droplet digital PCR

Digital PCR was performed on a QX100 droplet PCR system (Bio-Rad). PCR reactions were prepared as previously described (9, 21). Briefly, emulsified PCR reactions were run on a 96 well plate on a G-Storm GS4 thermal cycler incubating the plates at 95°C for 10 min followed by 40 cycles of 95°C for 15 sec, 60°C for 60 sec, followed by 10 min incubation at 98 °C. Plates were read on a Bio-Rad QX100 droplet reader using QuantaSoft v1.6.6.0320 software. Copy number variation and gene expression for target genes were calculated as a ratio with multiplexed reference genes (Supplementary Table 3). Copy number variation assays were performed using 1-3ng genomic DNA, aiming to obtain a 300-600 reference droplets.

For gene expression assays, cDNA was prepared using SuperScript® III First Strand kit (Life Technologies, 18080-051), according to the manufacturer's guidelines using 50-200ng total RNA primed with random hexamers. ddPCR gene expression reactions (Supplementary Table 3) were typically set up with 1-5ng RNA equivalent of cDNA. Target expression was normalized using βActin and GAPDH references assays.

In situ heterogeneity mapping

Briefly, fluorescent sections were scanned into the MIRAX (Pannoramic) scanner at high magnification in the x, y and z planes and analysed using custom HALO software. Tumour compartments were marked by a pathologist and the entire tumour area analysed for amplified and non-amplified tumour cells. Amplified cells were determined as those with a ratio *FGFR2:CEP10 >2*, and assessed only in cells with CEP10 signals ≥2. Percentage amplified tumour cells and total copy number was calculated. A manuscript describing *In situ* heterogeneity mapping is under preparation.

Nanostring

Probe sequences were custom designed and manufactured by Nanostring. Multiple probes were included against key genes including FGFR2. Probe specificity was confirmed using BLAT and Arrayviewer (Browser and Land software). The codeset was validated with cells lines and clinical tissue known to overexpress FGFR2. In addition to genes of interest the Codeset included a number of housekeeping genes to correct for RNA input amount and/or quality. A positive control (Universal Human Reference RNA (UHR), Stratagene, catalog #75000-41) was run routinely to ensure consistency between runs. Input total RNA amount was 100ng or 5ul neat RNA for more dilute/poor quality samples (based on internal QC control criteria).

Protocol was followed according to standard nCounter instructions. GEN2 Prep Station incubation time was set at the higher sensitivity setting (3hrs) and 280 Fields of View (FOV) were routinely captured unless otherwise noted.

Data was normalized through an internally developed Pipeline Pilot Tool (publicly available for use on the Comprehensive R Archive Network, CRAN). In brief, data were log2 transformed after being normalized in two steps: raw Nanostring counts were first background adjusted with a Truncated Poisson correction using negative control spikes followed by a technical normalization using positive control spikes. Data was then corrected for input amount variation through a Sigmoid shrunken slope normalization step using the mean expression of housekeeping genes. A transcript was designated as not detected if the raw count was below the average of the internal negative control raw counts plus 2 standard deviations.

siRNA screen

Screening in 384 well plates with a Dharmacon siGENOME SMART pools library targeting all known protein kinases and phosphatases as described previously (5). To assess the effect of siRNA on growth/survival, the effect of siRNA in the vehicle plates was expressed as a Z score, with the standard deviation estimated from the median absolute deviation (MAD). To assess the effect of siRNA on sensitivity to PD173074 the log2 ratio between growth in PD173074 plates and vehicle plates was assessed and expressed as a Z score.

Western Blotting

Cell lines were grown on 35mm plates, treated as indicated, and lysed in NP40 lysis buffer, (1% v/v NP40, 10mM Tris.Cl pH8, 150mM NaCl, 1mM EDTA, 1mM DTT) supplemented with phosphatase (5mM Na_4P_2O7, 50mM NaF and 1mM NaVO4) and protease inhibitor cocktail (Roche, 11697498001). Cells were reverse transfected with siRNA 72 hours prior to lysis. Western blots were carried out with precast TA or Bis-Tris gels (Life Technologies).

In vitro cell line assessment

Clonogenic assays were conducted in 6 well plates, with 1000 cells seeded per well, and 24 hours later cells exposed to vehicle, or the indicated treatments followed by growth in media for 2 weeks to allow colony growth. Colonies were fixed, stained with sulforhodamine B and counted. For PTEN siRNA clonogenics cells were treated for 1 week with PD173074 before wash out. For short-term survival assays, cells were exposed to indicated drugs with survival assessed after 72 hours exposure with Cell Titre-Glo cell viability assay (Promega, Madison, WI). To assess the effect of siRNA on drug sensitivity cells were reverse transfected at final siRNA concentration 20nM, at 48 hours post transfection plates were exposed to compound with survival was assessed after 72 hours exposure. To assess synergy cell lines were

plated in 384 well plates, and the following day exposed to fixed-ratio combinations of indicated drugs for 72 hours, with combination index assessed according to Chou and Talalay (22) using Calcusyn v2.1 (BIOSOFT, UK).

Whole Exome Sequencing

Genomic DNA (30-200ng) was fragmented to 200bp using a Covaris E Series and the resultant libraries were subjected to DNA Capture using SureSelect XT Human All Exon v4 kit (Agilent) following manufacturer's instructions. Final libraries were quantified using qPCR and clustered at a molarity of 14.5pM, sequencing was performed on an Illuimna HiSeq 2000 using 2x75 cycles of version 3 SBS chemistry. Reads were aligned to the human reference genome (GRCh37) using BWA (v0.7.5a) (23). PCR duplicates were filtered out from the subsequent analysis using Picard-tools (v1.94) and variants were called using the GATK pipeline (v2.3.9) best practices (24). Somatic changes between germline, cancer samples and the PDX samples were investigated using MuTect (v1.1.4) (25) and filtered for on-target regions using bedTools (v2.17.0) Comparisons between allele frequencies of somatic mutations in the cancer and PDX samples were investigated using R (3.1.2). All sequencing data has been deposited in the NCBI Sequence Read Archive under accession SRP072158**.**

Apoptosis assessment

To assess apoptosis activated Caspase 3/7 activity was assessed using the Caspase-Glo® 3/7 Assay according to manufacturer's instructions (Promega, G8090) and adjusted for cell number as assessed by Cell Titre-Glo.

Phosphorylated RTK arrays

Cells and PDX were treated as indicated, lysates prepared using Lysis Buffer 17 and analysed using Human Phospho-RTK arrays (R&D Systems, ARY001B) according to the manufacturer's guidelines.

Immunoprecipitation

Cells were treated as indicated and lysates prepared using NP40 lysis buffer (without DTT). The antibodies used for immunoprecipitation (IP) were p85 PI3K (ABS233, Millipore), ErbB3 (Thermo Scientific, MS-262-P1) and FGFR2 (Santa Cruz, SC122). Control IPs were performed with normal mouse (SC2025) and rabbit IgG (SC2027, both Santa Cruz Biotechnologies). Veriblot anti-rabbit IgG (ab131366) and anti-mouse IgG (ab131368, both Abcam) HRP conjugated secondary antibodies were used for IPs. 500-1000mg of total cellular protein were incubated with the antibodies and the protein complexes precipitated using Protein G coated Dynabeads (Life Technologies, 10001D).

Ras activation Assay

Ras activation was determined using the Ras activation assay kit (Millipore, 17-218) according to the manufacturer's guidelines. Briefly, cell lysates were prepared using Mg^{2+} Lysis/wash buffer (MLB). Samples were incubated with 10μg Ras assay reagent (Raf1 Ras binding domain-agarose) and incubated for 45min at 4˚C. Agarose beads were pelleted by centrifugation and washed 3 times with MLB. Agarose beads were resuspended in NuPAGE LDS sample buffer (Life Technologies). Samples were subjected to western blotting as previously described and blots probed using anti-Ras antibody (clone RAS10, 05-516, Millipore).

Methyl 7- GTP pull down

Cells were lysed in NP40 lysis buffer. Pulldown mixes were prepared with 200μL containing 200μg total cellular protein and 40μL 7methyl GTP-sepharose 4B beads (GE Healthcare, 275025) to give a total volume of 240μL. Before use beads were washed twice with NP40 lysis buffer. Pulldown mixes were incubated overnight at 4˚C. Beads were washed twice with NP40 lysis buffer, bound complexes eluted in western sample loading buffer and resolved on precast Bis-Tris gels (Life Technologies).

AHA translation assay

Protein synthesis was assessed using the Click IT AHA-Alexa Fluor 488 Protein Synthesis HCS Assay (Invitrogen C10289). L-azidohomoalanine (AHA) is an analog of methionine that contains an azide moiety. AHA that has been incorporated into proteins can be detected by ligation of a fluorescently labelled alkyne.

Cells were grown on coverslips for 2 days, the media changed and treated with 50nM AZD4547 for 24h. Experimental conditions were removed and the cells washed with methionine free RMPI media (Sigma, R7513). Cells were treated with AHA prepared according to the manufacturer's guidelines in methionine free RMPI media for 30mins. The AHA-media was removed, the cells washed twice with sterile cold PBS and the fixed with 4% paraformaldehyde (PFA). Coverslips were washed twice with 3%$^{w}/_{v}$ BSA in PBS and then permeabilised in 0.5% $^{v}/_{v}$ Triton-X100. Coverslips were washed before incubation with the Alexa Fluor 488 alkyne reaction mix for 30mins. Coverslips were washed and cells counterstained with Hoechst 33342. The coverslips were mounted onto glass slides with Vectastain (Vector, H1000). Fluorescently stained cells were imaged using an SP2 system Leica confocal microscope and images analysed using Adobe Photoshop Extended CS5.

Patient derived and cell line xenografts

All animal experiments were performed under a UK Home Office Project License assessed by ethical review committee.

Patient derived xenografts were established from fresh core biopsies collected into DMEM containing penicillin and streptomycin. Tissues samples were washed with 3 changes of DMEM containing antibiotics and implanted subcutaneously either on the flank or intra scapular of male Balb/c nude mice. Once tumours had established, they were collected, dissected and implanted into more male Balb/c nude mice for therapeutic experiments using AZD4547. Tumours were size matched and randomized to Control (Vehicle, 0.5% $^{w}/_{v}$ hydroxypropylmethylcellulose, 0.1% $^{v}/_{v}$ polysorbate 80 in water) or AZD4547 (5mg/Kg qd, in vehicle). Mice were dosed daily via oral gavage.

NCI-H1581 xenografts were generated by subcutaneous injection of $5x10^6$ cells in 50%$^{v}/_{v}$ Growth Factor Reduced Matrigel (BD Biosciences, 356231) in 40 Balb/c nude mice. After 7 days tumours were measured, size matched and the mice randomized to 4 experimental groups including Control (Vehicle), AZD4547 (5mg/Kg qd, in vehicle), AZD8055 (20mg/Kg qd, in vehicle) and AZD4547+AZD8055 (5mg/Kg qd and 20mg/kg qd respectively, in vehicle). Mice were dosed daily via oral gavage. Tumour size was assessed 3 times a week and expressed relative to the size at the start of treatment. To assess the signalling effect of the combinations mice with NCI-H1581 xenografts were dosed daily for 3 days. Mice were sacrificed 6 hours after the last treatment and tumours fixed with 4% paraformaldehyde in phosphate buffered saline.

Immunohistochemistry

Following deparafinisation and rehydration, antigen retrieval was, followed by blocking of endogenous peroxidise activity using H_2O_2 block (Dako Envision Flex kit, K8000).

For FGFR2 IHC, antigen retrieval was with pressure cooking in pH 9 retrieval buffer (DakoS2367). Sections were rinsed TBS-Tween 0.05% (TBS-T) and endogenous peroxidise blocked using H_2O_2 block (Dako Envision Flex kit, K8000). Sections were incubated for 1 hour with 1/10000 FGFR2 antibody (AZ AGG 2935-1C11, mouse monoclonal, from Astra Zeneca), followed by Envision+/HRP (Dako K4001) for 30 minutes and staining with DAB. Sections were washed and counterstained in Gills Haematoxylin

.

References

1. Turner N, Grose R. Fibroblast growth factor signalling: from development to cancer. Nat Rev Cancer. 2010;10:116-29.
2. Dieci MV, Arnedos M, Andre F, Soria JC. Fibroblast growth factor receptor inhibitors as a cancer treatment: from a biologic rationale to medical perspectives. Cancer Discov. 2013;3:264-79.
3. Gavine PR, Mooney L, Kilgour E, Thomas AP, Al-Kadhimi K, Beck S, et al. AZD4547: an orally bioavailable, potent, and selective inhibitor of the fibroblast growth factor receptor tyrosine kinase family. Cancer Res. 2012;72:2045-56.
4. Wolff AC, Hammond ME, Hicks DG, Dowsett M, McShane LM, Allison KH, et al. Recommendations for human epidermal growth factor receptor 2 testing in breast cancer: American Society of Clinical Oncology/College of American Pathologists clinical practice guideline update. J Clin Oncol. 2013;31:3997-4013.
5. Herrera-Abreu MT, Pearson A, Campbell J, Shnyder SD, Knowles MA, Ashworth A, et al. Parallel RNA interference screens identify EGFR activation as an escape mechanism in FGFR3-mutant cancer. Cancer Discov. 2013;3:1058-71.
6. Razzaque MS. The FGF23-Klotho axis: endocrine regulation of phosphate homeostasis. Nat Rev Endocrinol. 2009;5:611-9.
7. Cha JY, Maddileti S, Mitin N, Harden TK, Der CJ. Aberrant receptor internalization and enhanced FRS2-dependent signaling contribute to the transforming activity of the fibroblast growth factor receptor 2 IIIb C3 isoform. J Biol Chem. 2009;284:6227-40.
8. Ueda T, Sasaki H, Kuwahara Y, Nezu M, Shibuya T, Sakamoto H, et al. Deletion of the carboxyl-terminal exons of K-sam/FGFR2 by short homology-mediated recombination, generating preferential expression of specific messenger RNAs. Cancer Res. 1999;59:6080-6.
9. Gevensleben H, Garcia-Murillas I, Graeser MK, Schiavon G, Osin P, Parton M, et al. Noninvasive detection of HER2 amplification with plasma DNA digital PCR. Clin Cancer Res. 2013;19:3276-84.
10. Wang J, Wen S, Symmans WF, Pusztai L, Coombes KR. The bimodality index: a criterion for discovering and ranking bimodal signatures from cancer gene expression profiling data. Cancer Inform. 2009;7:199-216.
11. Cancer Genome Atlas Research N. Comprehensive molecular characterization of gastric adenocarcinoma. Nature. 2014;513:202-9.
12. Ong SH, Hadari YR, Gotoh N, Guy GR, Schlessinger J, Lax I. Stimulation of phosphatidylinositol 3-kinase by fibroblast growth factor receptors is mediated by coordinated recruitment of multiple docking proteins. Proc Natl Acad Sci U S A. 2001;98:6074-9.
13. Castellano E, Sheridan C, Thin MZ, Nye E, Spencer-Dene B, Diefenbacher ME, et al. Requirement for interaction of PI3-kinase p110alpha with RAS in lung tumor maintenance. Cancer Cell. 2013;24:617-30.
14. Ueki K, Algenstaedt P, Mauvais-Jarvis F, Kahn CR. Positive and negative regulation of phosphoinositide 3-kinase-dependent signaling pathways by three different gene products of the p85alpha regulatory subunit. Mol Cell Biol. 2000;20:8035-46.
15. Slamon DJ, Leyland-Jones B, Shak S, Fuchs H, Paton V, Bajamonde A, et al. Use of chemotherapy plus a monoclonal antibody against HER2 for metastatic breast cancer that overexpresses HER2. N Engl J Med. 2001;344:783-92.
16. Dowsett M, Procter M, McCaskill-Stevens W, de Azambuja E, Dafni U, Rueschoff J, et al. Disease-free survival according to degree of HER2 amplification for patients treated with adjuvant chemotherapy with or without 1 year of trastuzumab: the HERA Trial. J Clin Oncol. 2009;27:2962-9.
17. Wolff AC, Hammond ME, Hicks DG, Dowsett M, McShane LM, Allison KH, et al. Recommendations for human epidermal growth factor receptor 2 testing in breast cancer:

American Society of Clinical Oncology/College of American Pathologists clinical practice guideline update. J Clin Oncol. 2013;31:3997-4013.
18. Kunii K, Davis L, Gorenstein J, Hatch H, Yashiro M, Di Bacco A, et al. FGFR2-amplified gastric cancer cell lines require FGFR2 and Erbb3 signaling for growth and survival. Cancer Res. 2008;68:2340-8.
19. Lamont FR, Tomlinson DC, Cooper PA, Shnyder SD, Chester JD, Knowles MA. Small molecule FGF receptor inhibitors block FGFR-dependent urothelial carcinoma growth in vitro and in vivo. Br J Cancer. 2011;104:75-82.
20. Cunningham D, Allum WH, Stenning SP, Thompson JN, Van de Velde CJ, Nicolson M, et al. Perioperative chemotherapy versus surgery alone for resectable gastroesophageal cancer. N Engl J Med. 2006;355:11-20.
21. Garcia-Murillas I, Lambros M, Turner NC. Determination of HER2 amplification status on tumour DNA by digital PCR. PLoS One. 2013;8:e83409.
22. Chou TC. Drug combination studies and their synergy quantification using the Chou-Talalay method. Cancer Res. 2010;70:440-6.
23. Li H, Durbin R. Fast and accurate short read alignment with Burrows-Wheeler transform. Bioinformatics. 2009;25:1754-60.
24. McKenna A, Hanna M, Banks E, Sivachenko A, Cibulskis K, Kernytsky A, et al. The Genome Analysis Toolkit: a MapReduce framework for analyzing next-generation DNA sequencing data. Genome Res. 2010;20:1297-303.
25. Cibulskis K, Lawrence MS, Carter SL, Sivachenko A, Jaffe D, Sougnez C, et al. Sensitive detection of somatic point mutations in impure and heterogeneous cancer samples. Nat Biotechnol. 2013;31:213-9.

Figure Legends

Figure 1. Clinical activity of FGFR inhibitor AZD4547 in FGFR amplified breast and gastric cancer.

A. Waterfall plot from 12 patients with *FGFR1* amplified breast cancer or *FGFR2* amplified gastric cancer, with maximum change in tumour size (Y axis) and duration on study (yellow, Z axis). Red are patients with confirmed partial response. Five patients who progressed clinically are not shown.

B. Representative CT scans from baseline and 6 months in a patient with *FGFR2* amplified gastric cancer with a partial response in liver metastases (marked with white arrow on baseline scan).

C. 18F-FDG-PET scans from baseline (*top*) and day 15 (*bottom*) in patients who responded to AZD4547. *Left* 3 patients with *FGFR2* amplified gastric cancer, and *right* 1 patient with *FGFR1* amplified breast cancer. Red boxes mark abnormal areas of 18F-FDG uptake in baseline scan, and corresponding areas in the day 15 scan. Normal 18F-FDG uptake is seen in brain, heart, kidneys and bladder.

Figure 2. High-level clonal amplification of FGFR2 that predicts for sensitivity to FGFR inhibitor can be identified through ctDNA screening

A. *FGFR1* copy number and *FGFR2* copy number in breast and gastric cancers respectively assessed by digital PCR, from 17 patients treated with AZD4547. Red indicates patients who had a confirmed partial response to AZD4547, grey indicates patients with a partial metabolic change on day15 18F-FDG-PET but without a clinical response, and black patients without response. Response to AZD4547 is only seen in cancers with high-level copy number amplification (p=0.0026, Mann Whitney U Test), and partial metabolic change

in *FGFR2* amplified cancers is only seen in cancers with high-level copy number amplification (p=0.0022, Mann Whitney U Test).

B. FGFR2 mRNA expression assessed in baseline tumour biopsies by reverse transcription digital PCR *(left)*, with FGFR2 immunohistochemistry *(right)*, Colour coding as in part A. FGFR2 mRNA expression was normalized to reference genes βActin and GAPDH. Data is presented as the mean of the FGFR2:βActin and FGFR2:GAPDH ratios.

C. Assessment of clonality of *FGFR2* amplification by *FGFR2* FISH on tumour sections, assessed with automated MIRAX analysis, divided by cancers that demonstrated clinical response (269 and 316) and no clinical response. Percentage of tumour cells with amplification is displayed, along with representative image from MIRAX analysis colour coded by the presence of amplified tumour cells (red) and non-amplified tumour cells (blue). The presence of non-amplified tumour cells in patient 99 was confirmed visually.

D. Comparison of FGFR2 mRNA expression assessed by Nanostring™ in tumour biopsies from baseline and day 15. A substantial fall in FGFR2 expression is seen in the highly FGFR2 amplified but heterogeneous tumour from patient 135 potentially reflecting sub-clonal loss of FGFR2 over-expression tumour clone.

E. Analysis of *FGFR2* copy number in plasma DNA, from plasma samples taken at baseline. #, baseline plasma was not collected for patient 99, cfDNA was isolated from cycle1 day8 predose.

Figure 3. High-level FGFR2 amplified cell lines are highly sensitive to FGFR inhibition

A. *FGFR1* copy number and *FGFR2* copy number in a panel of 82 breast and 74 gastric tumours and cell lines (respectively). FGFR2 amplification has a bimodal distribution with a distinct highly amplified population (Bimodality index 2.74). Red indicates tumours with response to AZD4547 in the clinic, and light blue tumours that did not respond.

B. Western blot of cell lysates from FGFR driven cell lines, blotted for phospho-FGFR (Tyr653/654 on FGFR1), FGFR2, and βactin loading control.

C. Cell line panel was treated with PD173074 for 72 hours, with EC50 (*left*) and fractional kill at 1μM (*right*). *FGFR2* amplified cell lines have higher sensitivity compared to *FGFR1* cell lines (P=0.0087 and P=0.0109 respectively, Mann-Whitney U Test). MFM223 *PIK3CA* mutant cell line is indicated.

D. The panel of FGFR driven cell lines was treated with AZD4547 for 72 hours, *FGFR2* amplified cell lines had a lower EC50 than *FGFR1* amplified cell lines (p=0.0303, Mann-Whitney U Test).

E. Caspase 3/7 activity in the panel of *FGFR* driven cell lines was assessed in responses to treatment with 50nM AZD4547 for 24 hours and expressed relative to cells treated with vehicle. *FGFR2* amplified cells have a higher level of apoptosis (p=0.0357, Mann-Whitney U Test).

F. Patient derived xenografts were generated from baseline biopsies of two *FGFR2* amplified patients that responded to AZD4547 (FG51/pt269 and FG42/pt316). Xenografts were established in nude mice and divided randomly into 2 groups treated daily with vehicle and AZD4547 12.5mg/kg QD for 2 weeks. For both models, n=4 controls and n=5 AZD4547, *p<0.05 and ***p<0.001 2-way ANOVA.

G. Western blot of cleaved caspase 3 in lysates from FG42/pt316 PDXs treated with vehicle or AZD4547 12.5mg/kg QD for 28 hours, with tumours collected 4 hours post last dose of AZD4547.

Figure 4. Functional genomic screens reveal that PI3 kinase and mTOR signalling determines the sensitivity of FGFR2 amplified cell lines to FGFR inhibition

A. Supervised clustering of the effect of siRNA on sensitivity to PD173074 from parallel siRNA screens in FGFR driven cell lines, with the differential effect of siRNA according to *FGFR2* amplification status. Displayed are the top siRNA with a permutation p value <0.05 that increase (*top*) and decrease (*bottom*) sensitivity to PD173074. Full siRNA screen results are in Supplementary Fig. 4A.

B. Clonogenic survival assays in SUM52 transfected with siCON or siPTEN SMARTpool exposed to fixed doses of PD173074 as indicated or vehicle. Data presented as mean with SEM (n=3), ***p<0.001 2-way ANOVA.

C. Western blots of SUM52 cells transfected 72 hours earlier with siCON or siPTEN SMARTpool and treated with indicated doses of PD173074 or vehicle for 1 hour, and blotted for phospho-AKT S473, total AKT and PTEN

D. Western blot of a panel of *FGFR1* and *FGFR2* amplified cell lines treated for indicated times with PD173074 500nM, separated by driving *FGFR* event, blotted for phospho AKT S473 and total AKT, phospho ERK1/2 T202/Y204 and total ERK1/2.

E. Western blot of lysates from patient derived spheroid cultures treated with AZD4547 100nM or vehicle for 1 hour, probed for phosphorylated forms of FGFR, ERK1,2, AKT, S6, and 4EBP1.

F. Western blot of cell panel treated with AZD4547 50nM for 1h and blotted for phospho-4EBP1 T37/46, along with total protein and βactin loading control.

G. 7-methyl-GTP pull down in SUM52 treated with vehicle or AZD4547 for 1 hour, blotted with indicated 5'-cap complex members.

H. FGFR2 amplified cell line SUM52 was cultured in media containing azidohomoalanine and treated with and without 50nM AZD4547, relative fluorescence was normalized for cell

number. Data is presented as mean with standard deviation (n=5 experiments), *P*=0.0313 Wilcoxon matched pairs signed rank test.

Figure 5. Hyperactive FGFR2 in high level amplified cell lines signals to PI3 kinase indirectly through ERBB3 and IRS1/IGF1R

A. SUM52 lysates were immunoprecipitated with antibodies against p85 PI3K, FGFR2, or control IgG, and blotted as indicated.

B. Phospho-receptor tyrosine kinase array of SUM52 cells (*left*) and SNU16 cells (*right*) treated with PD173074 or control for 1 hour.

C. Phospho-receptor tyrosine kinase array (*left panel*) of patient derived xenograft FG42 (pt316) with vehicle or AZD4547 12.5mg/kg QD for 28 hours, with tumours collected 4 hours post last dose of AZD4547. Western blots (*right panel*) of lysates from FG42 (pt316) treated with AZD4547 as described, probed for phospho-HER2, phospho-ERBB3, phospho-FGFR, and total proteins as indicated.

D. SNU16 cells were treated with vehicle or 500nM PD173074, lysates immunoprecipitated with ERBB3 or control antibody, and blotted for FGFR2, ERBB3, and p85 PI3K.

E. Western blots of Snu16 (*left)* and SUM52 (*right*) cells grown in complete media were transfected 72 hours earlier with multiple siRNA targeting ERBB3 or siCON, blotted with indicated antibodies

F. SNU16 were treated with vehicle or PD170374 500nM for 1h and blotted for phospho-AKT T308 and S473, phospho-ERK 1/2 T202/Y204, phospho-IGF1R Y1135 and phospho-FGFR Y653/654) and total proteins as indicated.

G. SNU16 cells were treated with IGF1R inhibitor 250nM AEW541 for 1 hour and blotted for phospho-AKT S473, phospho-ERK1/2 T202/Y204, phospho-IGF1R Y1135, phospho-FGFR and total proteins as indicated.

H. SNU16 were treated with vehicle, PD170374 500nM or AEW541 250nM for 1hour, lysates were precipitated with RAF1 Ras binding domain, and blotted with pan-RAS antibody to assess the level of GTP bound RAS.

I. Lysates of SNU16 cells treated with 500nM PD173074, 250nM AEW541, or the combination were immunoprecipitated with a p85 PI3K antibody or control IgG and blotted for IRS1, ERBB3 and p85.

FIGURE 1

A

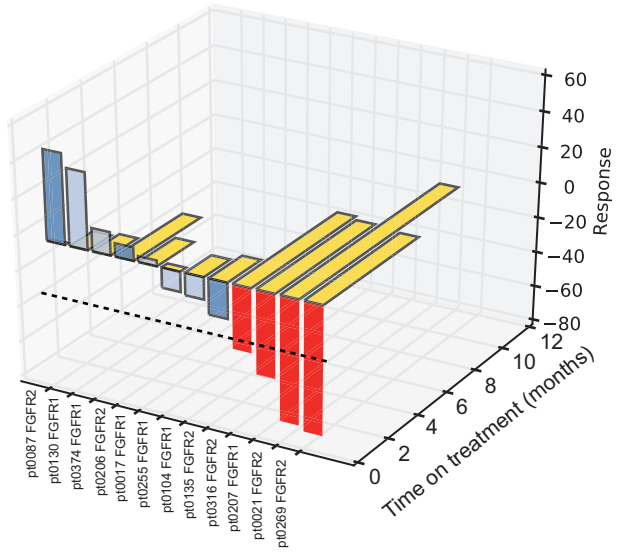
60
40
20
0
−20
−40
−60
−80
Response
0
2
4
6
8
10
12
Time on treatment (months)
pt0087 FGFR2
pt0130 FGFR1
pt0374 FGFR1
pt0206 FGFR2
pt0017 FGFR1
pt0255 FGFR1
pt0104 FGFR1
pt0135 FGFR2
pt0316 FGFR2
pt0207 FGFR1
pt0021 FGFR2
pt0269 FGFR2

B

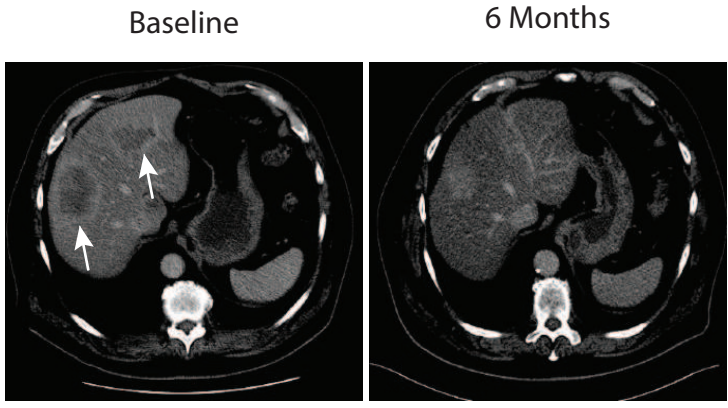
Baseline
6 Months

C

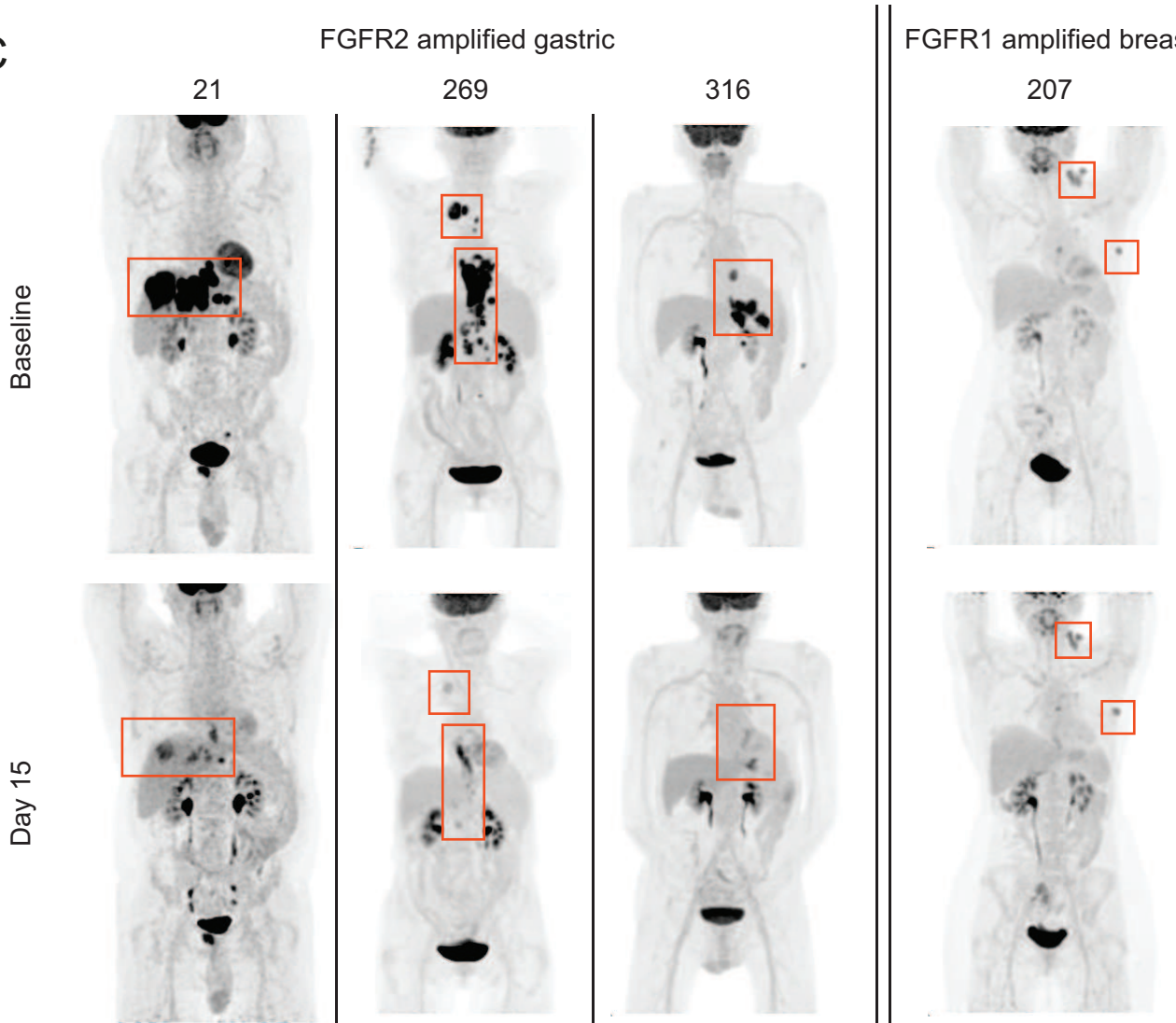
FGFR2 amplified gastric
FGFR1 amplified breast
21
269
316
207
Baseline
Day 15

FIGURE 2

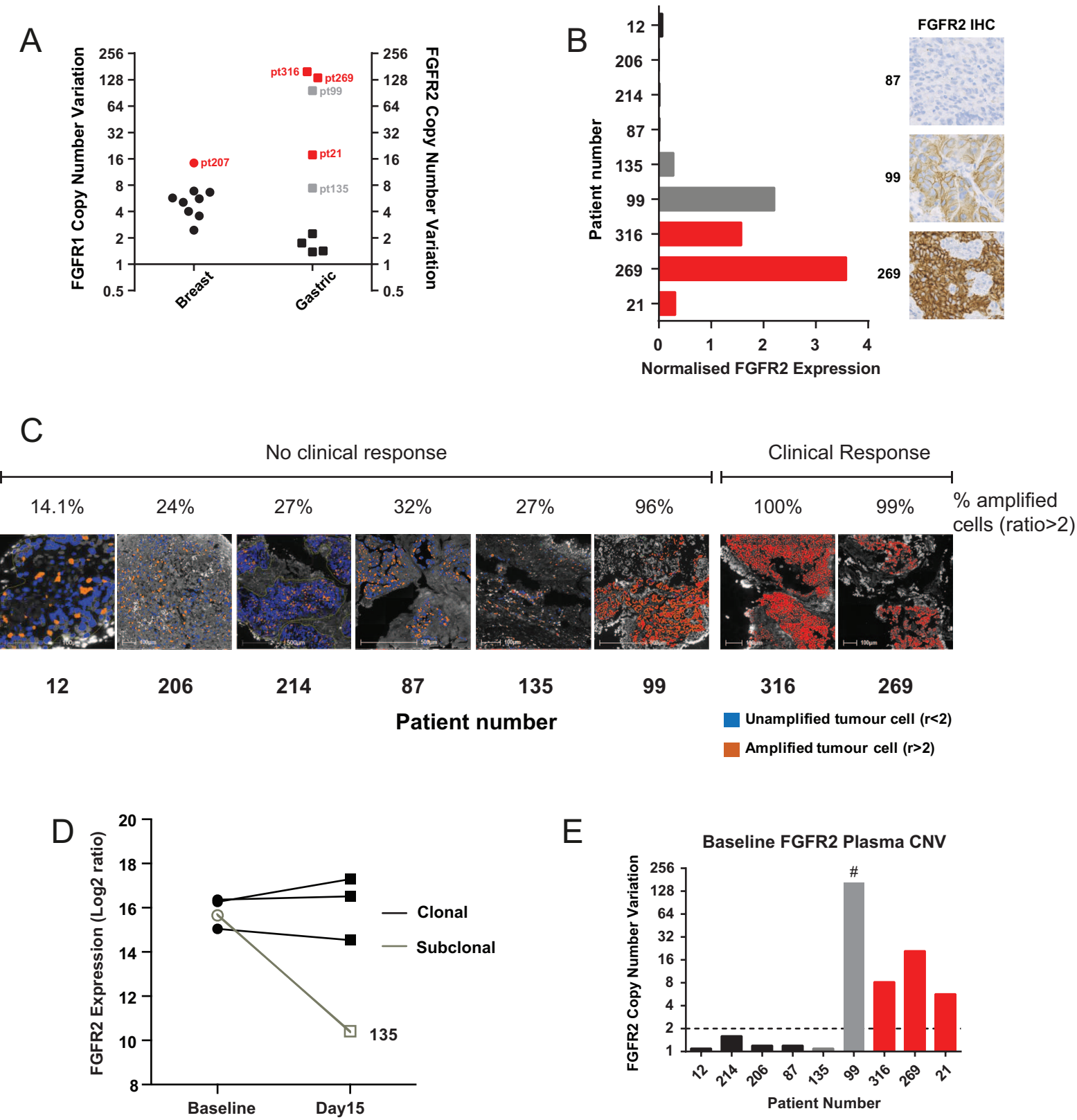
A
FGFR1 Copy Number Variation
FGFR2 Copy Number Variation
256
128
64
32
16
8
4
2
1
0.5
pt316
pt269
pt99
pt207
pt21
pt135
Breast
Gastric
B
Patient number
12
206
214
87
135
99
316
269
21
0
1
2
3
4
Normalised FGFR2 Expression
FGFR2 IHC
87
99
269
C
No clinical response
Clinical Response
14.1%
24%
27%
32%
27%
96%
100%
99%
% amplified cells (ratio>2)
12
206
214
87
135
99
316
269
Patient number
Unamplified tumour cell (r<2)
Amplified tumour cell (r>2)
D
FGFR2 Expression (Log2 ratio)
20
18
16
14
12
10
8
Clonal
Subclonal
135
Baseline
Day15
E
Baseline FGFR2 Plasma CNV
FGFR2 Copy Number Variation
256
128
64
32
16
8
4
2
1
#
12
214
206
87
135
99
316
269
21
Patient Number

FIGURE 3

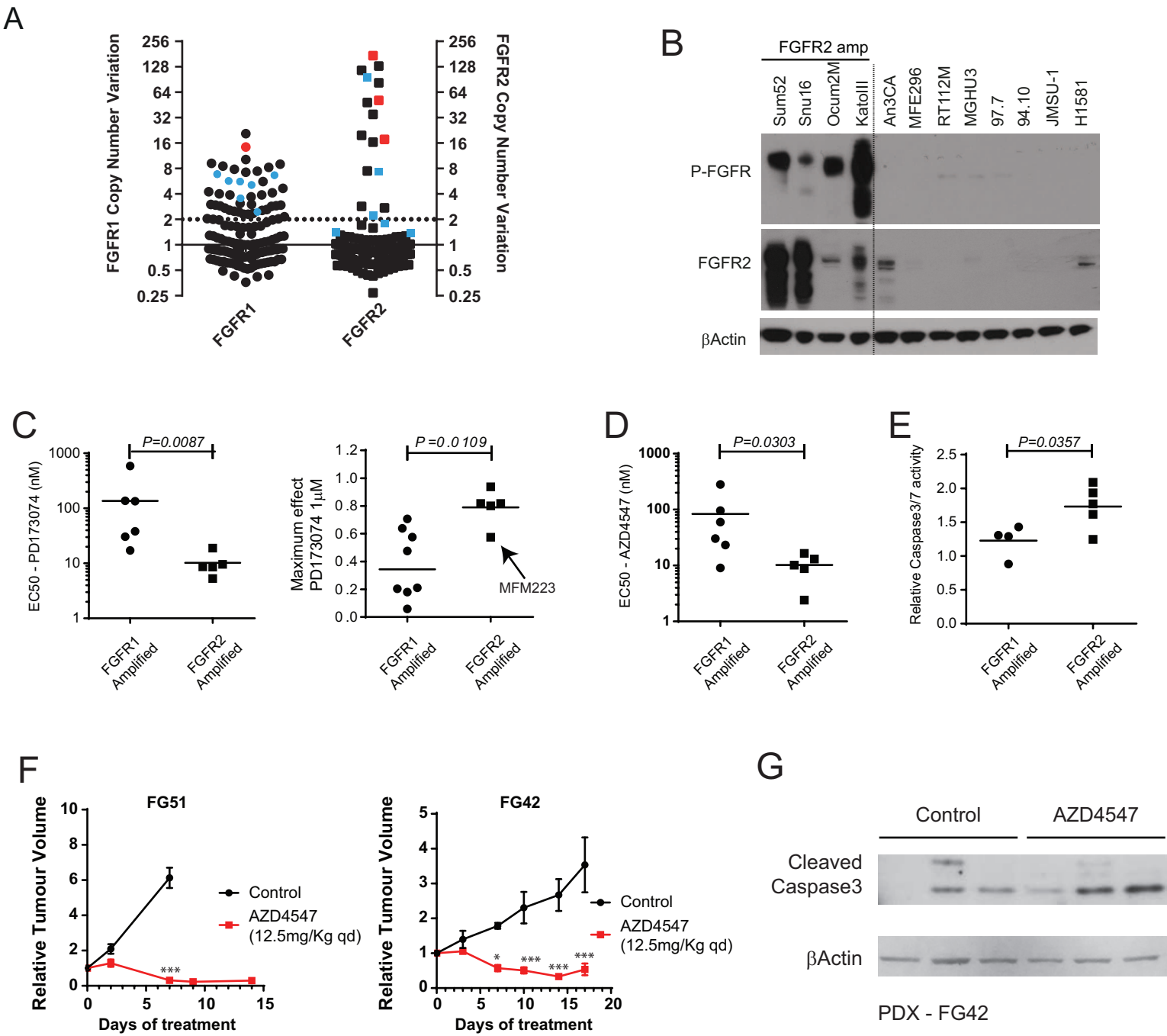
A
FGFR1 Copy Number Variation
FGFR2 Copy Number Variation
256
128
64
32
16
8
4
2
1
0.5
0.25
FGFR1
FGFR2
B
FGFR2 amp
Sum52
Snu16
Ocum2M
KatoIII
An3CA
MFE296
RT112M
MGHU3
97.7
94.10
JMSU-1
H1581
P-FGFR
FGFR2
βActin
C
P=0.0087
EC50 - PD173074 (nM)
1000
100
10
1
FGFR1 Amplified
FGFR2 Amplified
P =0.0109
Maximum effect PD173074 1μM
1.2
1.0
0.8
0.6
0.4
0.2
0.0
MFM223
D
P=0.0303
EC50 - AZD4547 (nM)
E
P=0.0357
Relative Caspase3/7 activity
2.5
2.0
1.5
1.0
0.5
0.0
F
FG51
FG42
Relative Tumour Volume
Days of treatment
Control
AZD4547
(12.5mg/Kg qd)
***
*
G
Control
AZD4547
Cleaved Caspase3
βActin
PDX - FG42

FIGURE 4

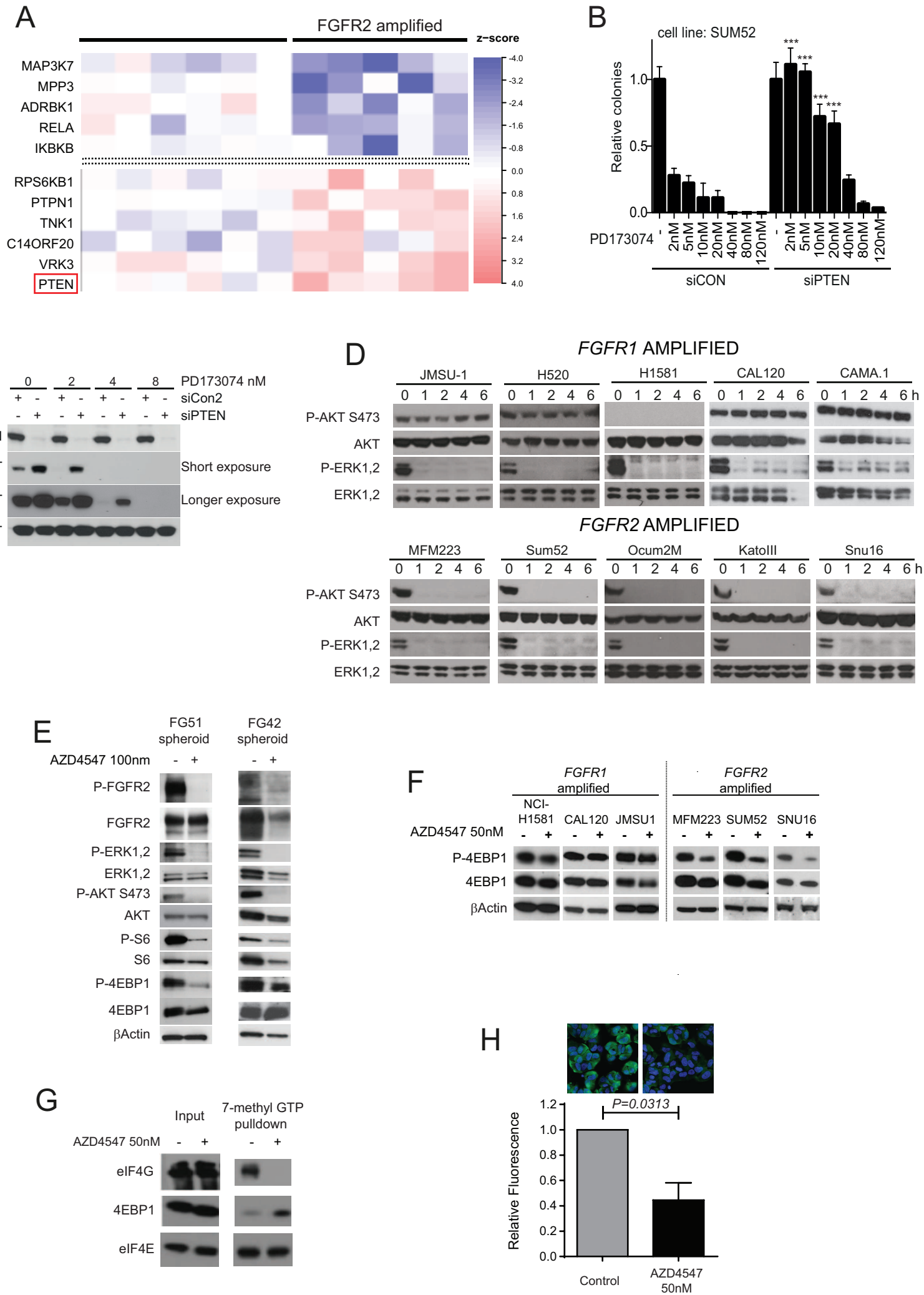
A
FGFR2 amplified
z-score
MAP3K7
MPP3
ADRBK1
RELA
IKBKB
RPS6KB1
PTPN1
TNK1
C14ORF20
VRK3
PTEN
B
cell line: SUM52
Relative colonies
PD173074
siCON
siPTEN
C
PD173074 nM
siCon2
siPTEN
PTEN
P-AKT
Short exposure
Longer exposure
AKT
D
FGFR1 AMPLIFIED
JMSU-1
H520
H1581
CAL120
CAMA.1
P-AKT S473
AKT
P-ERK1,2
ERK1,2
FGFR2 AMPLIFIED
MFM223
Sum52
Ocum2M
KatoIII
Snu16
E
FG51 spheroid
FG42 spheroid
AZD4547 100nm
P-FGFR2
FGFR2
P-ERK1,2
ERK1,2
P-AKT S473
AKT
P-S6
S6
P-4EBP1
4EBP1
βActin
F
FGFR1 amplified
FGFR2 amplified
NCI-H1581
CAL120
JMSU1
MFM223
SUM52
SNU16
AZD4547 50nM
P-4EBP1
4EBP1
βActin
G
Input
7-methyl GTP pulldown
AZD4547 50nM
eIF4G
4EBP1
eIF4E
H
P=0.0313
Relative Fluorescence
Control
AZD4547 50nM

FIGURE 5

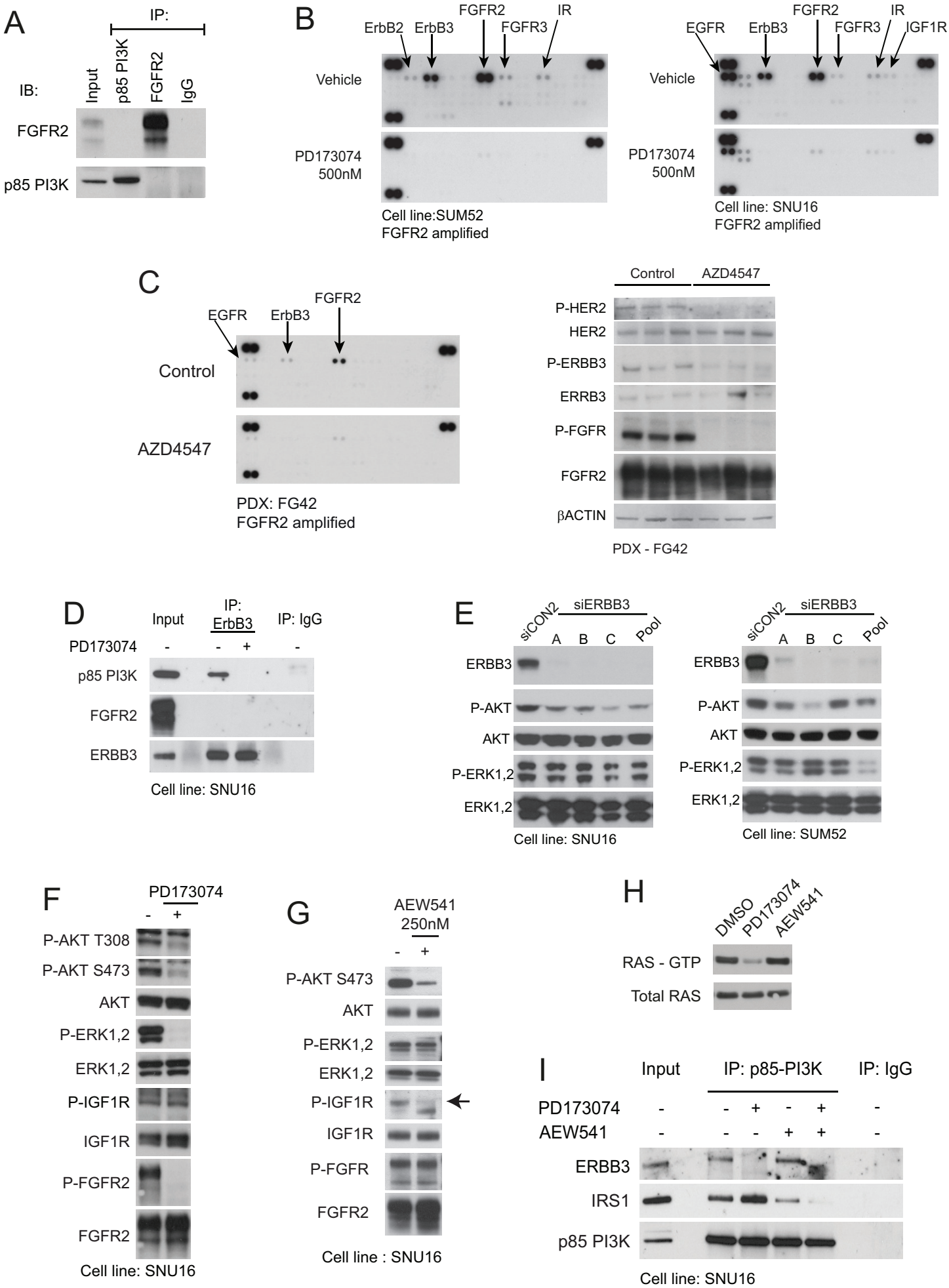
A
IP:
IB:
Input
p85 PI3K
FGFR2
IgG
FGFR2
p85 PI3K
B
ErbB2
ErbB3
FGFR2
FGFR3
IR
Vehicle
PD173074
500nM
Cell line:SUM52
FGFR2 amplified
EGFR
ErbB3
FGFR2
FGFR3
IR
IGF1R
Vehicle
PD173074
500nM
Cell line: SNU16
FGFR2 amplified
C
EGFR
ErbB3
FGFR2
Control
AZD4547
PDX: FG42
FGFR2 amplified
Control
AZD4547
P-HER2
HER2
P-ERBB3
ERRB3
P-FGFR
FGFR2
βACTIN
PDX - FG42
D
Input
IP: ErbB3
IP: IgG
PD173074
p85 PI3K
FGFR2
ERBB3
Cell line: SNU16
E
siCON2
siERBB3
A
B
C
Pool
ERBB3
P-AKT
AKT
P-ERK1,2
ERK1,2
Cell line: SNU16
Cell line: SUM52
F
PD173074
P-AKT T308
P-AKT S473
AKT
P-ERK1,2
ERK1,2
P-IGF1R
IGF1R
P-FGFR2
FGFR2
Cell line: SNU16
G
AEW541
250nM
P-AKT S473
AKT
P-ERK1,2
ERK1,2
P-IGF1R
IGF1R
P-FGFR
FGFR2
Cell line : SNU16
H
DMSO
PD173074
AEW541
RAS - GTP
Total RAS
I
Input
IP: p85-PI3K
IP: IgG
PD173074
AEW541
ERBB3
IRS1
p85 PI3K
Cell line: SNU16